Precision Tests of the Nonlinear Mode Coupling of Anisotropic Flow via High-Energy Collisions of Isobars

Jiangyong Jia (贾江涌)[1,2*], Giuliano Giacalone[3*], and Chunjian Zhang(张春健)[1]

[1]*Department of Chemistry, Stony Brook University, Stony Brook, NY 11794, USA*
[2]*Physics Department, Brookhaven National Laboratory, Upton, NY 11976, USA*
[3]*Institut für Theoretische Physik, Universität Heidelberg, Philosophenweg 16, 69120 Heidelberg, Germany*

(Received 14 December 2022; accepted manuscript online 27 February 2023)

Valuable information on dynamics of expanding fluids can be inferred from the response of such systems to perturbations in their initial geometry. We apply this technique in high-energy ^{96}Ru+^{96}Ru and ^{96}Zr+^{96}Zr collisions to scrutinize the expansion dynamics of the quark-gluon plasma, where the initial geometry perturbations are sourced by the differences in deformations and radial profiles between ^{96}Ru and ^{96}Zr, and the collective response is captured by the change in anisotropic flow V_n between the two collision systems. Using a transport model, we analyze how the nonlinear coupling between lower-order flow harmonics V_2 and V_3 to the higher-order flow harmonics V_4 and V_5, expected to scale as $V_{4\mathrm{NL}} = \chi_4 V_2^2$ and $V_{5\mathrm{NL}} = \chi_5 V_2 V_3$, gets modified as one moves from ^{96}Ru+^{96}Ru to ^{96}Zr+^{96}Zr systems. We find that these scaling relations are valid to high precision: variations of order 20% in $V_{4\mathrm{NL}}$ and $V_{5\mathrm{NL}}$ due to differences in quadrupole deformation, octupole deformation, and nuclear skin modify χ_4 and χ_5 by about 1–2%. Percent-level deviations are however larger than the expected experimental uncertainties and could be measured. Therefore, collisions of isobars with different nuclear structures are a unique tool to isolate subtle nonlinear effects in the expansion of the quark-gluon plasma that would be otherwise impossible to access in a single collision system.

DOI: 10.1088/0256-307X/40/4/042501

The space-time evolution of the quark-gluon plasma (QGP) produced in high-energy nuclear collisions is driven by pressure-gradient forces that convert spatial deformations in the initial geometry into momentum-space deformations that are captured by azimuthal correlations among final-state hadrons.[1–3] These correlations emerge in the Fourier spectrum of the azimuthal particle distribution, $p(\phi) \propto \sum_{n=-\infty}^{\infty} V_n e^{in\phi}$.[4] The dissipative effects in the QGP expansion quickly dampen the V_n spectrum as one goes higher in n.[5] The dominant coefficients, reflecting genuine deformations of the QGP geometry, are elliptic flow, V_2, and triangular flow, V_3. Damped higher harmonics are strongly affected by their couplings to V_2 and V_3. Quadrangular flow, V_4, for instance, receives a large contribution from its coupling to V_2, which scales as V_2^2.

Over the past decade, many theoretical[5–17] and experimental[18–22] investigations have clarified the mechanism by which V_2 and V_3 source harmonics of higher order. The resulting picture is that $V_{n,n>3}$ contains a contribution reflecting a genuine n^{th}-order deformation, denoted as $V_{n\mathrm{L}}$, plus a contribution from couplings to V_2 and V_3, denoted as $V_{n\mathrm{NL}}$. For V_4 and V_5, the decompositions are[9]

$$V_4 = V_{4\mathrm{L}} + \chi_4 (V_2)^2, \qquad V_5 = V_{5\mathrm{L}} + \chi_5 V_2 V_3, \tag{1}$$

from which we define the nonlinear parts as $V_{4\mathrm{NL}} = \chi_4 (V_2)^2$, $V_{5\mathrm{NL}} = \chi_5 V_2 V_3$. The coefficient χ_4, for example, determines the coupling strength between the elliptic and quadrangular flow. Measurements of these couplings are of great interest as they are dynamically generated during the QGP expansion. They probe the transport and hadronization properties of the QGP, whose characterization is one of the main goals of high-energy heavy-ion collision experiments.

This paper establishes a new method to probe the nonlinear coupling of flow harmonics in the QGP expansion. We look at two collision systems at identical multiplicities but with small differences in their initial geometries. We study how the QGP responds to such differences in the dynamically generated couplings between V_2 and V_3, and between higher-order harmonics V_4 and V_5. We argue that the cleanest method to achieve this is to exploit isobars. These are nuclei with identical mass numbers but different deformations and radial profiles, providing the desired differences in collision geometries. We focus on ^{96}Ru+^{96}Ru and ^{96}Zr+^{96}Zr collisions, for which high-precision experimental data are available from the Relativistic Heavy Ion Collider (RHIC).[23] Using a transport model, we predict χ_n in these two systems, and systematically address the impact of nuclear structure on such observables. The χ_n show very small differences between ^{96}Ru+^{96}Ru and ^{96}Zr+^{96}Zr, much smaller than the calculated differences for corresponding nonlinear terms $V_{n\mathrm{NL}}$. These small differences are ascribed to subleading nonlinear couplings, so far undetected in heavy-ion collisions, which are within the reach of the existing isobar data. We conclude that the different structures of two isobars can be exploited as a precision tool to access subtle nonlinear phenomena in the QGP expansion.

*Corresponding authors. Email: jiangyong.jia@stonybrook.edu; giulianogiacalone@gmail.com
© 2023 Chinese Physical Society and IOP Publishing Ltd

Model, Observables, Goal. We study ^{96}Ru+^{96}Ru and ^{96}Zr+^{96}Zr collisions within the Glauber Monte Carlo model.[24] The colliding ions are treated as collections of nucleons that are randomly distributed in each event according to a Woods–Saxon density,

$$\rho(r,\theta,\phi) \propto \frac{1}{1+e^{[r-R_0(1+\beta_2 Y_2^0(\theta,\phi)+\beta_3 Y_3^0(\theta,\phi))]/a_0}}, \quad (2)$$

with four nuclear structure parameters: nuclear diffusivity a_0, half-width radius R_0, quadrupole deformation β_2, and octupole deformation β_3. Each collision has a number of nucleons that participate in the interaction, which gives rise to the QGP. The evolution of QGP is modeled via the multi-phase transport code (AMPT),[25] version v2.26t5 in string-melting mode, which generates the hadrons in the final state. Observables are calculated using hadrons with $0.2 < p_{\rm T} < 2\,{\rm GeV}$ for events sorted in intervals of $N_{\rm ch}$: the charged hadron multiplicity for $p_{\rm T} > 0.1\,{\rm GeV}$ and $|\eta| < 0.5$, similar to the experiment.[23] The observables of interest involve products of flow vectors $V_n = v_n e^{in\Psi_n}$ averaged over events with the same $N_{\rm ch}$, where Ψ_n is the orientation of the harmonic and $v_n \equiv |V_n|$ is its amplitude. Such averages are computed within the framework of multi-particle correlations.[26,27] In particular, we use a sub-event method[28] by correlating particles in the pseudorapidity window $0 < \eta < 2$ with those having $-2 < \eta < 0$ to reduce the impact of non-collective (non-flow) correlations.

Our focus is on ratios of observables taken between ^{96}Ru+^{96}Ru and ^{96}Zr+^{96}Zr collisions. We study the dynamical response of the QGP to small differences in the initial geometry induced by the nuclear structure. The V_2 and V_3 emerge as a response to the initial spatial deformations (or eccentricities) $\mathcal{E}_2$ and $\mathcal{E}_3$,[3] respectively. The response coefficient $K_n = V_n/\mathcal{E}_n$ is a probe of the medium properties, and has been investigated in model studies of isobar collisions.[29–31] Here, we look instead at the coupling between harmonics represented by χ_n. The advantage of such quantities is that they do not directly depend on eccentricities [Eq. (3)], and can be extracted directly from experimental V_n data.

To this end, we continue from the decompositions in Eq. (1). Defining $V_{n\rm L}$ as the vector that is uncorrelated with $V_{n\rm NL}$ in the considered event class,[9] $\langle V_{4\rm L}(V_2^*)^2\rangle = \langle V_{5\rm L}V_2^*V_3^*\rangle = 0$, one obtains an unique expression for the coupling coefficients,

$$\chi_4 = \frac{\langle V_4(V_2^2)^*\rangle}{\langle v_2^4\rangle}, \qquad \chi_5 = \frac{\langle V_5(V_2V_3)^*\rangle}{\langle v_2^2 v_3^2\rangle}. \quad (3)$$

It is clear that both χ_4 and χ_5 are expressed in terms of quantities that are measurable. By construction, the χ_n encodes as well the effect of subleading couplings that go beyond the V_2^2 or V_2V_3 terms. If the impact of such subleading couplings becomes more visible as we vary the initial geometry, then χ_n would change accordingly. The goal of this work is to expose and make a precision test of this feature using collisions of isobars, which permits us to claim evidence of subleading couplings in V_4 and V_5, driven by small differences in the initial geometry between ^{96}Ru+^{96}Ru and ^{96}Zr+^{96}Zr collisions.

The same could in principle be achieved by comparing other species at the same multiplicities, for instance, ^{238}U+^{238}U versus ^{197}Au+^{197}Au or ^{208}Pb+^{208}Pb versus ^{129}Xe+^{129}Xe, collisions that have already been taken at RHIC and the Large Hadron Collider (LHC), respectively. However, as the expected contribution from subleading modes to χ_n is small, it may be beyond the genuine measurement systematics. In contrast, the isobar running mode guarantees that ratios of observables are devoid of measurement systematics,[32] as well as system dependence of final state effects,[33] which makes the extraction of novel nonlinear effects possible.

Nonlinear Coupling Coefficients. To make progress, we perform the exercise recently proposed in Refs. [17,34]. We denote by $\mathcal{R}_{\mathcal{O}}$ the ratio of observable $\mathcal{O}$ taken between ^{96}Ru+^{96}Ru and ^{96}Zr+^{96}Zr collisions at fixed $N_{\rm ch}$,

$$\mathcal{R}_{\mathcal{O}}(N_{\rm ch}) = \frac{\mathcal{O}_{\rm Ru+Ru}(N_{\rm ch})}{\mathcal{O}_{\rm Zr+Zr}(N_{\rm ch})}. \quad (4)$$

We shall refer to such operation as the *isobar ratio*. Taking the isobar ratio of the plane correlators $\langle V_4(V_2^2)^*\rangle$ and $\langle V_5V_2^*V_3^*\rangle$ yields

$$\mathcal{R}_{\langle V_4(V_2^*)^2\rangle} = \mathcal{R}_{\chi_4}\mathcal{R}_{\langle v_2^4\rangle}, \quad \mathcal{R}_{\langle V_5V_2^*V_3^*\rangle} = \mathcal{R}_{\chi_5}\mathcal{R}_{\langle v_2^2 v_2^3\rangle}. \quad (5)$$

The ratio at the same $N_{\rm ch}$ ensures a nearly perfect cancelation of final state effects for flow observables due to, e.g., viscosity and hadronization.[33] One also in general expects that χ_n are nearly independent of initial-state features, i.e., $\mathcal{R}_{\chi_n} \approx 1$.[9] Therefore, the ratio of the plane correlators should be given by the ratio of $\langle v_2^4\rangle$ or $\langle v_2^2 v_3^2\rangle$, which in turn are directly influenced by the nuclear structure parameters. To see this explicitly, we simulate generic high-statistics isobar collisions for several choices of Woods–Saxon densities listed in Table 1, which were found to describe ratios of several observables in isobar collisions.[30] These permit us to isolate the impact of individual features of the nuclear profiles. For instance, Case1/Case2 isolates the impact of β_2, while the combined effect of all four parameters is reflected by Case1/Case5.

Figure 1 shows the $N_{\rm ch}$ dependence of the ratios in Eq. (5), including the impact of the four Woods–Saxon parameters one at a time. The top row shows results for V_4. Remarkably, we see that the ratio of plane correlators $\mathcal{R}_{\langle V_4(V_2^2)^*\rangle}$ follows very precisely $\mathcal{R}_{\langle v_2^4\rangle}$, irrespective of the source of modifications in the nuclear structure induced to v_2. Within the precision of this plot, $\mathcal{R}_{\chi_n} = 1$ is confirmed. This result reproduces nicely the preliminary measurement of this observable by the STAR collaboration.[35] It is interesting to note that the $\mathcal{R}_{\langle v_2^2\rangle^2}$ (open diamonds) also follows very closely the $\mathcal{R}_{\langle v_2^4\rangle}$, with a visible difference appearing only after a change in surface diffuseness, a_0. This behavior can be understood from the following identity,

$$\mathcal{R}_{\langle v_2^2\rangle^2} - \mathcal{R}_{\langle v_2^4\rangle} = x(\mathcal{R}_{v_2\{4\}^4} - \mathcal{R}_{\langle v_2^4\rangle}),$$
$$x \equiv v_2\{4\}^4/(2\langle v_2^2\rangle^2),$$

where we have introduced the fourth-order cumulant of the fluctuations of v_2: $v_2\{4\}^4 = 2\langle v_2^2\rangle^2 - \langle v_2^4\rangle$. In the top-middle panel of Fig. 1, a quick estimate gives $x \sim 0.1$ and $\mathcal{R}_{v_2\{4\}^4} \sim 1.35$ in mid-central collisions, which explains quantitatively why $\mathcal{R}_{\langle v_2^2\rangle^2}$ is about 2% larger than $\mathcal{R}_{\langle v_2^4\rangle}$.

The lower panels of Fig. 1 display similar comparisons for V_5. Our conclusions are unchanged. In this case, we predict in addition perfect agreement between the ratio of $\langle v_2^2 v_3^2\rangle$ and that of $\langle v_2^2\rangle\langle v_3^2\rangle$ for all Woods–Saxon parameters. This is expected from the rather weak correlation between v_2 and v_3 in heavy ion collisions. [19,36–38]

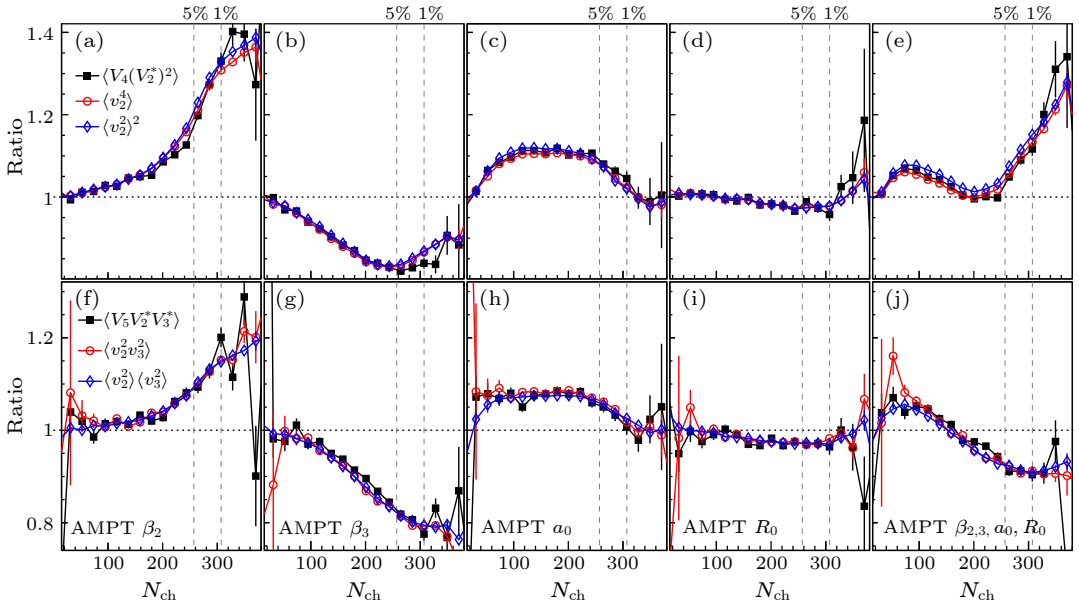

Fig. 1. Isobar ratios of $\langle V_4(V_2^*)^2\rangle$, $\langle v_2^4\rangle$, $\langle v_2^2\rangle^2$ [(a)–(e)], and $\langle V_5 V_2^* V_3^*\rangle$, $\langle v_2^2 v_3^2\rangle$, $\langle v_2^2\rangle\langle v_3^2\rangle$ [(f)–(j)]. We consider the impact of β_2, β_3, a_0, R_0, and all of them are included, moving from left to right in the figure. The locations for 1% and 5% most central collisions are indicated by vertical dashed lines.

Table 1. Woods–Saxon parameters for ^{96}Ru (Case1), ^{96}Zr (Case5). The three other cases allow us to study the impact of nuclear structure on observables step by step. About 170 million AMPT events are generated for each case, about 10% of the available real isobar data for one collision system. The choice of parameters is motivated by previous comparisons between AMPT results and experimental data. [30]

	R_0 (fm)	a_0 (fm)	β_2	β_3
Case1 ^{96}Ru	5.09	0.46	0.162	0
Case2	5.09	0.46	0.06	0
Case3	5.09	0.46	0.06	0.20
Case4	5.09	0.52	0.06	0.20
Case5 ^{96}Zr	5.02	0.52	0.06	0.20
Ratios	$\frac{\text{Case1}}{\text{Case2}}$,	$\frac{\text{Case2}}{\text{Case3}}$,	$\frac{\text{Case3}}{\text{Case4}}$,	$\frac{\text{Case4}}{\text{Case5}}$,	$\frac{\text{Case1}}{\text{Case5}}$

Having exposed the nonlinear couplings, we zoom in on these curves and examine the actual values of $\mathcal{R}_{\chi_n}$. Our predictions are given in Fig. 2. We do observe small systematic deviations of up to 1–2% level induced by nuclear structure effects. Concerning χ_4, the most significant deviations are associated with the nuclear deformation parameters β_2 and β_3. Larger β_2 in ^{96}Ru leads to a slight decrease of χ_4 from peripheral to central collisions, while the larger β_3 of ^{96}Zr leads to the opposite effect. Similar effects are observed for χ_5. The effects are largest in central collisions, where the impact of the β_n are significant, and therefore any difference in the hydrodynamic response between isobars would be more visible. Both ratios are, on the other hand, more weakly dependent on the radial profile parameters a_0 and R_0.

The insets of Fig. 2 show our predictions for χ_4 and χ_5 as a function of $N_{\rm ch}$. They exhibit a weak centrality dependence, with only a decrease in the 0–5% centrality range, consistent with recent STAR measurement [22] in ^{197}Au+^{197}Au collisions. We stress that the precision reached in our analysis is in fact worse than what could be achieved based on the datasets available to the STAR collaboration. Therefore, percent level deviations could be easily detected with the isobar data.

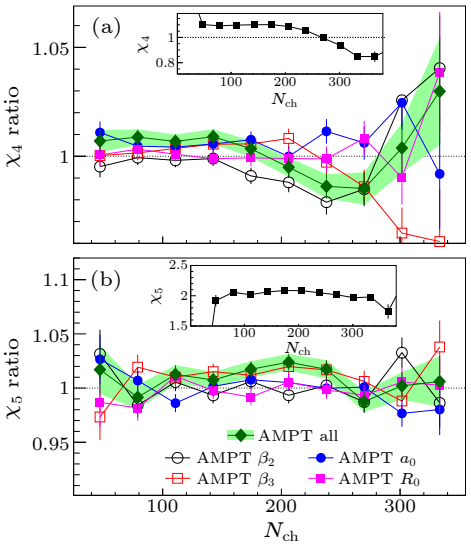

Fig. 2. Isobar ratios of nonlinear response coefficients χ_4 (a) and χ_5 (b) as a function of $N_{\rm ch}$. The impact of various Woods–Saxon parameters is exhibited separately, as well as combined together. The insets show predictions for χ_4 and χ_5 averaged over all cases.

This leads us to our main conclusion. The fact that $\mathcal{R}_{\chi_n} \neq 1$ implies the presence of additional nonlinear contributions to V_4 and V_5, driven by the nuclear structure effects. For instance, an important nonlinear contribution to V_4 beyond V_2^2 should be V_3V_1. It makes sense, then, that χ_4 is affected by the large β_3 in ^{96}Zr, as both V_1 and V_3 have a leading dependence on β_3.[39] However, since both V_1 and V_3 do not have a leading dependence on β_2, the dependence of $\mathcal{R}_{\chi_4}$ on β_2 suggests another nonlinear contribution, potentially in the form of $V_3^2V_2^*$ (In principle, the nonlinear mode $V_1^2V_2$ is also allowed. However, the p_T-integrated V_1 is known to be very small.[40] Thus, due to the presence of V_1^2, this mode should be strongly suppressed.). A detailed study of such geometry-induced subleading couplings is beyond the scope of this paper. However, this analysis can be readily performed if our prediction is confirmed by the experimental measurements. We emphasize once more that, without resorting to isobar ratios, it would be impossible to achieve the precision required to detect such effects. This is a remarkable consequence of the isobar collision campaign, with profound implications for future precision QGP studies.

Subleading Nonlinear Modes in v_{4L}. In the framework of nonlinear coupling coefficients, the definition of the nonlinear term $V_{n\mathrm{NL}}$ (and therefore χ_n) and the linear term $V_{n\mathrm{L}}$ are intertwined. This implies that, if χ_n coefficients are impacted by subleading nonlinear modes, such effect may also occur for $v_{n\mathrm{L}}$ and show up in the isobar ratio of $v_{n\mathrm{L}}$. We focus here on $n = 4$.

The linear component can be isolated by combing Eq. (1) with a two-particle measurement of V_4, $v_4\{2\}^2 \equiv \langle v_4^2 \rangle$,[18,19]

$$v_{4\mathrm{L}}^2 = v_4\{2\}^2 - v_{4\mathrm{NL}}^2, \qquad v_{4\mathrm{NL}}^2 \equiv \chi_4^2 \langle v_2^4 \rangle. \tag{6}$$

The isobar ratios of the three quantities in the above equation are related via a simple identity,

$$\mathcal{R}_{v_4\{2\}^2} = \mathcal{R}_{v_{4\mathrm{L}}^2} + (\mathcal{R}_{v_{4\mathrm{NL}}^2} - \mathcal{R}_{v_{4\mathrm{L}}^2})r, \quad r \equiv \frac{v_{4\mathrm{NL}}^2}{v_4\{2\}^2},$$
$$\mathcal{R}_{v_4\{2\}} \approx \mathcal{R}_{v_{4\mathrm{L}}} + (\mathcal{R}_{v_{4\mathrm{NL}}} - \mathcal{R}_{v_{4\mathrm{L}}})r. \tag{7}$$

The second line of the above equation is valid when all ratios are close to unity. Figure 3 shows our predictions for the isobar ratio of v_4, as well as how the impact of nuclear structure manifests in the linear, $v_{4\mathrm{L}}$, and nonlinear mode, $v_{4\mathrm{NL}}$, extracted using Eq. (6). Figure 3(a) displays the ratio $\mathcal{R}_{v_4\{2\}}$, which reveals small but rather complex dependencies on the nuclear structure parameters. Figure 3(c) shows the impact of such parameters on the nonlinear component, which we already observed from $\mathcal{R}_{\langle v_2^4 \rangle}$ in the top panels of Fig. 1 (however, note that $\mathcal{R}_{v_{4\mathrm{L}}} \approx \sqrt{\mathcal{R}_{\langle v_2^4 \rangle}}$). The fraction of nonlinear contribution, shown in the inset, approaches zero in central collisions so that $v_{4\mathrm{NL}}$ impacts $\mathcal{R}_{v_4\{2\}}$ mostly in the non-central region.

Figure 3(b) shows the ratio of linear modes, $\mathcal{R}_{v_{4\mathrm{L}}}$. We observe something important. The coefficient χ_4 in Fig. 2 shows a sensitivity to β_2 and β_3. The same does not occur for $v_{4\mathrm{L}}$, which can be understood from the fact that fourth-order eccentricity $\mathcal{E}_4$ does not depend on β_2 and β_3.[39] On the other hand, $v_{4\mathrm{L}}$ is more strongly impacted by the radial profile parameters, a_0 and R_0. These results imply that the effect of subleading modes to $v_{4\mathrm{L}}$ is complementary to that observed for $v_{4\mathrm{NL}}$. Both observables probe such phenomena but respond to initial-state deformations in different ways. We stress, once more, that all these features can be accessed experimentally via high statistics isobar data.

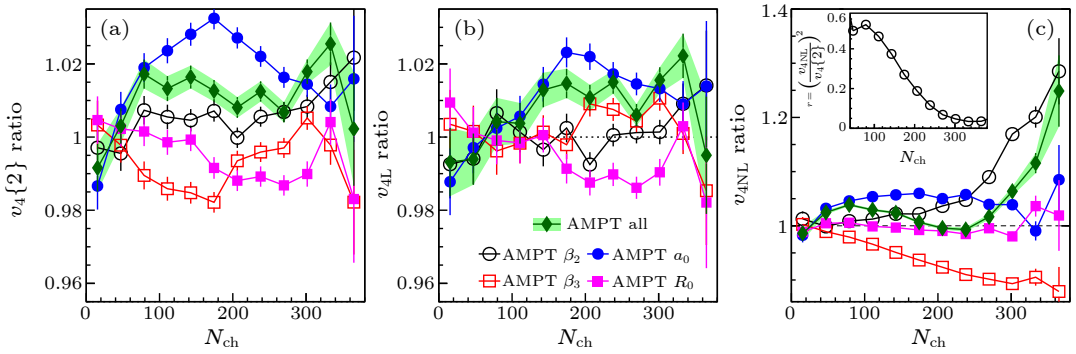

Fig. 3. The ratios of quadrangular flow from a two-particle method, $v_4\{2\}$ (a), and the ratios of estimated linear component, $v_{4\mathrm{L}}$ (b), and nonlinear component, $v_{4\mathrm{NL}}$ (c), as a function of N_{ch} in isobar collisions. Nuclear structure differences follow Table 1. The inset shows the fraction of v_4^2 carried by the nonlinear mode.

Conclusion and Prospects. Detailed transport simulations predict that the precision reached in the isobar ratios of higher-order flow harmonic coefficients permits one to scrutinize the effect of subleading couplings to V_4 and potentially V_5. If this prediction is confirmed in experiments, it will establish isobar collisions as a unique tool to study subleading nonlinear effects in the QGP expansion, exposed by the different structures of the two isobars. The largest subleading modes to V_4 should come from V_1V_3 and $V_3^2V_2^*$, namely,

$$V_4 = V_{4\mathrm{L}} + \chi_{4,22}V_2^2 + \chi_{4,31}V_1V_3 + \chi_{4,332}V_3^2V_2^*. \tag{8}$$

A self-consistent framework to define both $V_{4\mathrm{L}}$ and the coupling coefficients in the presence of multiple nonlinear components has been derived in Ref. [15], and could be readily applied to isobar data analysis. So far, subleading couplings have only been discussed in the analysis of V_6, V_7, V_8in ^{208}Pb+^{208}Pb collisions at LHC energies. The

rich nonlinear structure of, e.g., V_6 is, however, difficult to fully clarify via isobar ratios in ^{96}Ru+^{96}Ru and ^{96}Zr+^{96}Zr collisions at RHIC, as multiplicities are not high enough. If larger isobar pairs are collided in the future, potentially at higher collision energies at the LHC, such a possibility will be realized. Note that identification of nonlinear effects via isobar ratios allows cancelation of model uncertainties, which is not possible by looking at one collision system such as ^{208}Pb+^{208}Pb at the LHC. Therefore, isobar collisions will permit us to access experimentally the full intricacies of the nonlinear hydrodynamic response, thus opening a new promising opportunity for data-driven determinations of the QGP transport properties.

Acknowledgments. This research of J.J. and C.Z. is supported by DOE DE-FG02-87ER40331. The research of G.G. is funded by the Deutsche Forschungsgemeinschaft (DFG, German Research Foundation) under Germanys Excellence Strategy EXC2181/1-390900948 (the Heidelberg STRUCTURES Excellence Cluster), within the Collaborative Research Center SFB1225 (ISOQUANT, Project-ID 273811115). We acknowledge Somadutta Bhatta for their useful comments.

References

[1] Ollitrault J Y 1992 *Phys. Rev. D* **46** 229
[2] Alver B and Roland G 2010 *Phys. Rev. C* **81** 054905
[3] Teaney D and Yan L 2011 *Phys. Rev. C* **83** 064904
[4] Heinz U and Snellings R 2013 *Ann. Rev. Nucl. Part. Sci.* **63** 123
[5] Teaney D and Yan L 2012 *Phys. Rev. C* **86** 044908
[6] Gardim F G, Grassi F, Luzum M, and Ollitrault J Y 2012 *Phys. Rev. C* **85** 024908
[7] Teaney D and Yan L 2014 *Phys. Rev. C* **90** 024902
[8] Gardim F G, Noronha-Hostler J, Luzum M, and Grassi F 2015 *Phys. Rev. C* **91** 034902
[9] Yan L and Ollitrault J Y 2015 *Phys. Lett. B* **744** 82
[10] Qian J, Heinz U W, and Liu J 2016 *Phys. Rev. C* **93** 064901
[11] Giacalone G, Yan L, Noronha-Hostler J, and Ollitrault J Y 2016 *Phys. Rev. C* **94** 014906
[12] Qian J and Heinz U 2016 *Phys. Rev. C* **94** 024910
[13] Giacalone G, Yan L, Noronha-Hostler J, and Ollitrault J Y 2017 *J. Phys.: Conf. Ser.* **779** 012064
[14] Qian J, Heinz U, He R, and Huo L 2017 *Phys. Rev. C* **95** 054908
[15] Giacalone G, Yan L, and Ollitrault J Y 2018 *Phys. Rev. C* **97** 054905
[16] Magdy N 2022 *J. Phys. G* **49** 015105
[17] Zhao S, Xu H J, Liu Y X, and Song H 2022 arXiv:2204.02387 [nucl-th]
[18] Aad G, Abbott B, Abdallah J *et al.* (ATLAS collaboration) 2014 *Phys. Rev. C* **90** 024905
[19] Aad G, Abbott B, Abdallah J *et al.* (ATLAS collaboration) 2015 *Phys. Rev. C* **92** 034903
[20] Acharya S, Adamová D, Adolfsson J *et al.* (ALICE collaboration) 2017 *Phys. Lett. B* **773** 68
[21] Acharya S, Adamová D, Adler A *et al.* (ALICE collaboration) 2020 *J. High Energy Phys.* 2020(05) 085
[22] Adam J, Adamczyk L, Adams J R *et al.* (STAR collaboration) 2020 *Phys. Lett. B* **809** 135728
[23] Abdallah M S, Aboona B E, Adam J *et al.* (STAR collaboration) 2022 *Phys. Rev. C* **105** 014901
[24] Miller M L, Reygers K, Sanders S J, and Steinberg P 2007 *Ann. Rev. Nucl. Part. Sci.* **57** 205
[25] Lin Z W, Ko C M, Li B A, Zhang B, and Pal S 2005 *Phys. Rev. C* **72** 064901
[26] Bilandzic A, Snellings R, and Voloshin S 2011 *Phys. Rev. C* **83** 044913
[27] Bilandzic A, Christensen C H, Gulbrandsen K, Hansen A, and Zhou Y 2014 *Phys. Rev. C* **89** 064904
[28] Jia J Y, Zhou M L, and Trzupek A 2017 *Phys. Rev. C* **96** 034906
[29] Zhang C J and Jia J Y 2022 *Phys. Rev. Lett.* **128** 022301
[30] Jia J and Zhang C 2023 *Phys. Rev. C* **107** L021901
[31] Nijs G and van der Schee W 2021 arXiv:2112.13771 [nucl-th]
[32] Adam J, Adamczyk L, Adams J R *et al.* (STAR collaboration) 2021 *Nucl. Sci. Tech.* **32** 48
[33] Zhang C, Bhatta S, and Jia J 2022 *Phys. Rev. C* **106** L031901
[34] Magdy N 2022 arXiv:2206.05332 [nucl-th]
[35] Zhang C (STAR Collabration) 2022 *Observation of Nuclear Deformation in Isobar Colli Sions*, in *Proceedings of 29th International Conference on Ultra-Relativistic Nucleus-Nucleus Collisions*, 4–10 April 2022, Kraków, Poland
[36] Lacey R A, Reynolds D, Taranenko A, Ajitanand N N, Alexander J M, Liu F H, Gu Y, and Mwai A 2016 *J. Phys. G* **43** 10LT01
[37] Huo P, Jia J, and Mohapatra S 2014 *Phys. Rev. C* **90** 024910
[38] Adam J, Adamová D, Aggarwal M M *et al.* (ALICE collaboration) 2016 *Phys. Rev. Lett.* **117** 182301
[39] Jia J 2022 *Phys. Rev. C* **105** 014905
[40] Aad G, Abbott B, Abdallah J *et al.* (ATLAS collaboration) 2012 *Phys. Rev. C* **86** 014907